2021

# Combination of Local Heat Transfer and Flow Visualization of R245fa Flow Boiling in plate Heat Exchanger

Abdel-Rahman Farraj
*ACRC, the University of Illinois, Urbana, Illinois, USA*, afarraj2@illinois.edu

Pega Hrnjak
*ACRC, the University of Illinois, Urbana, Illinois, USA*

# Combination of Local Heat Transfer and Flow Visualization of R245fa Flow Boiling in Plate Heat Exchanger

Abdel-Rahman Farraj[1]*, Pega Hrnjak[1,2]*

[1]ACRC, the University of Illinois, Urbana, Illinois, USA

[2]Creative Thermal Solutions, Inc., Urbana, Illinois, USA

* Corresponding author: pega@illinois.edu

## ABSTRACT

This paper presents an experimental study of the local heat transfer coefficient in evaporation and simultaneous flow visualization in plate heat exchangers. The fluid used is R245fa. The temperature profile, local heat flux, and heat transfer coefficient are measured and calculated along the plate using an internally developed heat flux meter. The flux meter is built from two original plates with thermocouples soldered to their surface and sandwiched with a thermal infill material in between. After calibrating the flux meter to determine its local thermal resistance, the flux meter is assembled in a three-channel setup to measure the heat transfer from one side while visualizing the evaporating R245fa from the other. To visualize two-phase flow, we substituted one inner plate and one end plate with transparent replicated plates. The experimental results focus on the complete evaporation of saturated R245fa by heating water placed vertically with ascending flow. The results also discuss the effect of mass fluxes between 10-20 kg/m$^2$s in a 60° chevron angle commercial plate heat exchanger. The measured data showed that the average heat transfer coefficient increases with mass flux except, which is also indicated from the local values. The approach relates local heat transfer with flow regime within a plate channel while preserving the real geometry and operating condition, creating fundamentals for improving geometry.

## 1. INTRODUCTION

Plate heat exchangers (PHE) are widely used nowadays in many heat transfer industrial applications, including the HVAC, used as evaporators or condensers. The corrugated patterns in these heat exchangers provide a high heat transfer area per volume and contribute to the distribution of the flow for better thermal-hydraulic performance. Other advantages over the tubular or shell-and-tube heat exchangers are their flexibility, compactness, and uncomplicated structural support. In literature, most experimental studies on the heat transfer coefficient (HTC) of the PHE were performed based on the mean heat transfer performance by considering the streams' inlet and outlet readings. However, few experimental studies attempted to obtain local heat transfer measurements, and their methods are summarized below.

Freund and Kabelec (2010) utilized the temperature oscillation IR thermography (TOIRT) to measure the local HTC. Exterior radiant heat from laser or halogen spotlights is applied to a surface of the test section formed by two plates and one flow of fluid. IR camera is also used for surface temperature measurements. The HTC is calculated by timing the corresponding temperature response measured by IR thermography. Their technique showed a discontinuous pattern of HTC, with the lowest values at the contact points and lines of the maximum along the corrugation paths in PHE. The ratio of maximum and minimum HTC decreases with increasing Reynolds number. Overall, the averaged HTC agreed well with the previous correlation proposed in the same conditions. This work was done on a single-phase flow until the same group introduced their technique in two-phase flow. Grabenstein and Kabelac (2012) tested the TOIRT method on one channel flow with R365mfc as a working fluid. A visualization study was presented in a different test section by preserving the original geometry of the one channel PHE. The transparent part was replicated using a commercial steel plate from polyurethane. Film, bubbly, and slug flow were defined in the proposed flow regime map. Also, heat transfer and pressure drop correlations were developed and assigned to each flow regime.

Gherasim et al. (2011a) run experiments for a two-channel setup while measuring the endplates' outside wall temperature using 40 thermocouples. Temperature profiles are plotted by interpolating the temperature readings used to be validated with the CFD model. The model was developed to indicate the mass distribution inside the channel (Gherasim *et al.*, 2011b). The irregular isotherms showed a large temperature gradient in both lengthwise and widthwise directions of the endplate.

Arima *et al.* (2010) developed a worthy example of combining the local heat transfer and flow visualization. Wall temperature measurements were conducted using 22 thermocouples attached inside the heating frame, which is used to calculate the heat flux. The test section was a 2-channel setup investigating flow boiling of ammonia/water binary mixture. In the same test section, and the other side (adiabatic side), three transparent viewing areas were installed to provide flow visualization. The effect of vapor quality, mass flux, and heat flux were investigated, and the influence of flow pattern on heat transfer was observed. However, the presented experiment setup was conducted in flat plates, different than the corrugated designs on the geometry of the PHEs.

The IR thermography method was also used by Solotych *et al.* (2016); applied for the single-phase flow of HFE1700. The test section was one upward flow channel composed of two calcium fluoride plates. The plates were machined for the corrugation shapes and specific distributors to uniform the flow before going through the channel. An adaptive thin layer of carbon dispersed polyamide provides electrical heating to the refrigerant flow. The wall temperature was measured using a high-resolution infrared camera and, while the fluid temperature was measured using thermocouples at the inlet and outlet. Vakili-Farahan *et al.* (2014) used the same method to investigate the flow boiling of R345fa. Six areas with the exact dimensions between the inlet and outlet ports were machined into the PVC plates to measure surface temperature using IR-camera. The quasi-local pressure was calculated from the measurements of the saturation temperature from the six areas. Their work concluded that the two-phase behavior in PHEs is similar to the flow in pipes. Moreover, the flow distribution at the inlet and outlet zones of the PHEs influences the overall hydraulic and thermal performance.

The studies mentioned above showed methods of measuring the thermal performance inside the PHE. However, most of these methods do not reflect a real situation for industrial PHEs. External electrical heaters provide uniform heating that does not represent the heat flux distribution caused by the corresponding channels' heating fluid. Moreover, a machined corrugated surface with an external distributor does not represent the real plate channel's flow distribution. The inlet and outlet distribution area designs are essential in influencing flow and heat performance. Besides, few works used their methods to measure the HTC for two-phase flow.

Moreover, the heat transfer mechanism during the flow boiling is strongly dependent on the flow regimes. Consequently, visualization techniques are also essential to understand the fundamentals of heat transfer mechanisms. Different approaches were developed to visualize the two-phase flow in PHEs, despite the complex geometry of the PHEs. Hsieh *et al.* (2002) visualized the flow boiling of R-134a in one channel using an acrylic plate. For the same mass flux, a higher heat flux caused a more massive bubble at the departure zones. Their results also showed the influence of the mass flux on the bubble size was noticeable. At subcooling zones, a small, separated bubble was observed. As the subcooling condition reaches the saturated temperature, the bubbles start to merge and move vigorously.

Jassim *et al.* (2001) performed an investigation on adiabatic pressure drop and flow visualization for three different PHE geometries. The corrugated shape was machined on a transparent PVC plate and stacked together to form a PHE-similar flow channel. The light was provided by the reflection of a stroboscope from a white background for uniformity. As a result, four flow regimes (bubbly, rough annular, smooth annular, and mist) were observed and mapped out on a mass flux versus a quality basis for each geometry. Pressure drop was found to have a strong linear relationship with the kinetic energy per unit volume.

Lin's group studied the visualization and heat transfer for R134a in different test sections. Three-channel setup for the heat transfer measurement during a two-channel setup for the flow visualization. A transparent acrylic plate was machined and polished to substitute an endplate. A thin liquid film was observed, and flow was dominated by evaporation at the liquid-vapor interface (Yan and Lin, 1999). Severe nucleate boiling was spotted near the inlet port. During a subcooled boiling, bubbles were suppressed by increasing the mass flux and inlet subcooling (Hsieh *et al.*, 2002). The heat flux showed a large effect on the bubble concentration, coalesce, and generation frequency.

Different techniques were introduced for local heat transfer coefficient measurements and flow visualizations. However, there is no technique to simultaneously couple local heat transfer with flow visualization while preserving the real geometry and conditions. It is desirable to visualize how evaporating flow changes its flow regime while investigating the thermal performance using heating fluid. Therefore, this paper presents a technique introduced by Jin & Hrnjak (2017) to measure the local HTC and visualize the PHE flow. The effect of mass fluxes is discussed employing this method.

## 3. EXPERIMENTAL METHODOLOGY

### 3.1 Plate Geometry

The geometry of the frame-and-plate heat exchanger tested is depicted in Figure 1(a). It is an industrial 1pass-1pass U-type configuration having a chevron pattern with sinusoidal corrugations. The parameters of its geometry are also shown in Figure 1(a). The plates from the original PHE are reduced to four plates, i.e., three channels. The refrigerant R245fa is evaporating vertically upward in the central channel. The other two outer channels allow downward heating water, as shown in Figure 1(c).

### 3.2 Heat Flux Meter Plate

Since the plates' geometry is preserved, the refrigerant channel's one-sided plate is being substituted with the heat flux meter (HFM). It is considered of two original plates stacked to each other with an infill material between them. Each plate contains forty-four thermocouples soldered to its inner surface with the same location. The temperature distribution of each side will be interpolated between the measured values. The calibrated thermal resistance of the infill material is used to calculate the conductive heat flux from the water channel. The locations of the soldered thermocouples on the plates' inner side are shown in Figure 1(a). After fixing their exact locations, the epoxy infill is added to the corrugations' valleys, as shown in Figure 1(b) to hold the thermocouples wires and avoid any air bubbles at the bottom. Then other layers of epoxy are poured to fill the desired gap between the plates. The epoxy thickness is controlled by aluminum strips surrounding the heating area before pressing the two plates together.

The other sided plate of the refrigerant channel will permit visualization access to the flow regime. Therefore, this plate is being substituted with a transparent plate made of a clear polycarbonate sheet, as shown in Figure 1(d). The flat sheet was heated in an oven to a temperature of 140°C for deforming. Then pressed on the original stainless steel plate to replicate the original shape. The endplate in Figure 1(e) corresponding to the transparent sheet is replaced with an opaque resin plate to allow the visualization to penetrate the water channel.

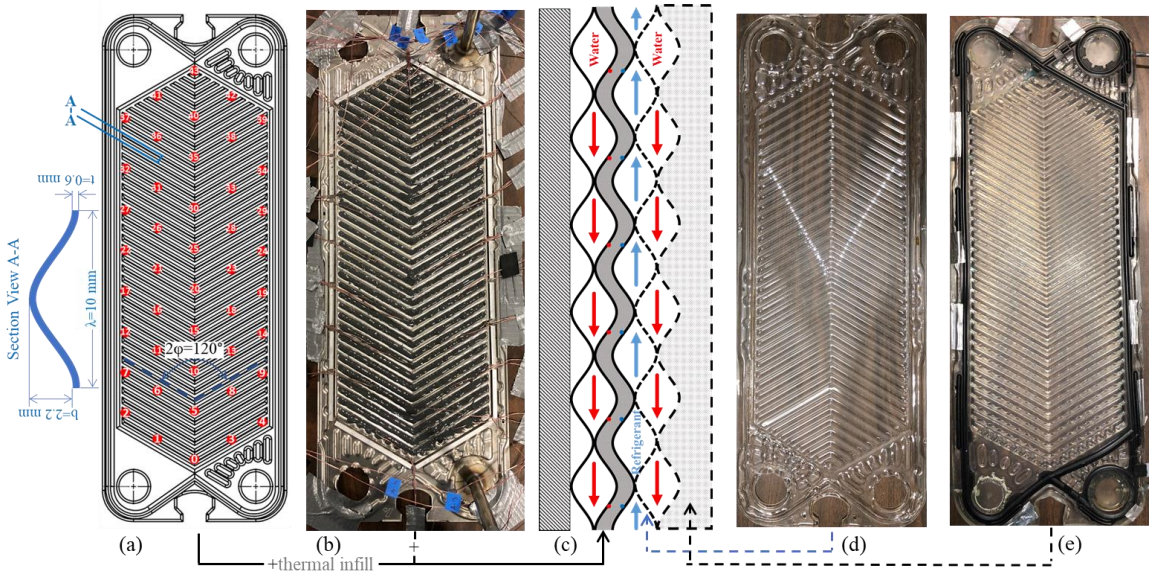


**Figure 1:** Components of the test section: (a) geometry of the plate and location of thermocouples (b) one side of HFM with thermal infill (c) cross section of the assembly (d) transparent inner plate (e) endplate resin.

For the refrigerant channel to gain equivalent heat from both sides of the heating water, the two-sided plates' thermal resistance should be the same. Therefore, the epoxy thickness inside the HFM is controlled according to the thickness of polycarbonate and both materials' thermal conductivity: polycarbonate and epoxy. The polycarbonate thickness is chosen to be 0.76 mm to optimize between the high temperature of water and the accuracy of the HFM.

### 3.3 Calibration of HFM

The eighty-eight thermocouples wires inside the infill material will cause non-uniform distribution of thermal conductivity inside the HFM. Additionally, the thickness could be varying in the middle region, away from the stripped aluminum. Also, the exact location of the measuring temperature from the soldering point could deviate from the required spot. Therefore, the local thermal resistance of HFM should be known to use the HFM as a sensor in the experiment.

Uniform electrical heat flux is applied to the HFM, and by measuring the local temperature from both sides, the local thermal resistance is obtained. Two methods were used with different spreaders between the heat source and the HFM. The first method used sand as a spreader because it provides conformal contact with the corrugation surface. The other side was left to be cooled by natural convection of air. The second method used water as a spreader of heat. The other side was cooled by controlling the temperature using an iced-water bath. The second method provided a higher heat flux in a range of the fluxes applied to the experimental tests.

The plate's heated area is divided into 64 segmented triangular regions according to the thermocouples' location, as shown in Figure 2. Each region's thermal resistance is calculated independently. The plate temperature of each region is the average of three-edged thermocouple readings. The distribution of thermal resistance was found by considering a range of heat flux (50-550 W) and is presented in Figure 3. Figure 4 shows the variation of the thermal resistance calculated for the 64 segmented areas at different heat fluxes. It shows a deviation of ±5% from the average value considered in the distribution map of Figure 3.

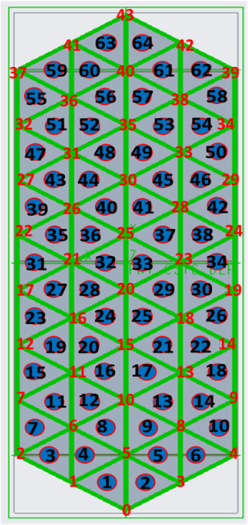

**Figure 2:** Divided heated area

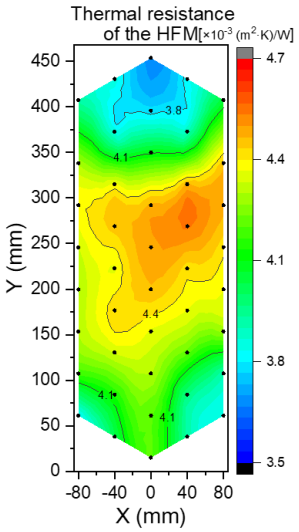


**Figure 3:** Distribution map of thermal resistance of HFM

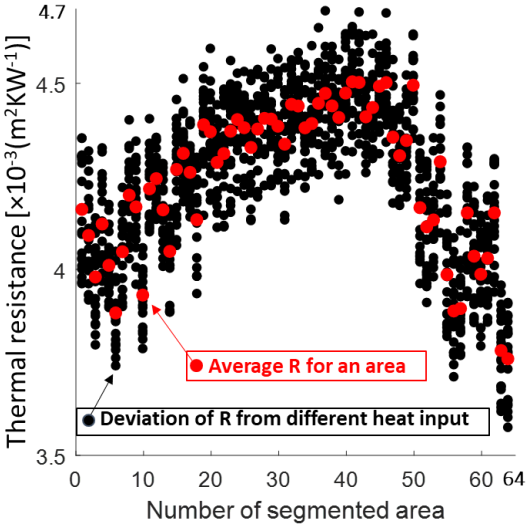


**Figure 4:** Variation of calculated thermal resistance of 64 areas at different heat fluxes

## 4. EXPERIMENTAL APPARATUS AND PROCEDURE

The schematics of the experimental apparatus is shown in Fig 5. It consists of three independent loops: refrigerant loop, water loop for heating, and water-glycol loop for cooling. The tested refrigerant mass flow rate is controlled by a magnetically driven pump and preheated by an electrical heater before entering the test section. The water stream provides the desired heat in the test section by controlling its mass flow rate and inlet temperature in the water loop. The outlet refrigerant from the test section is being cooled in the condenser and subcooled heat exchangers with the water-glycol loop.

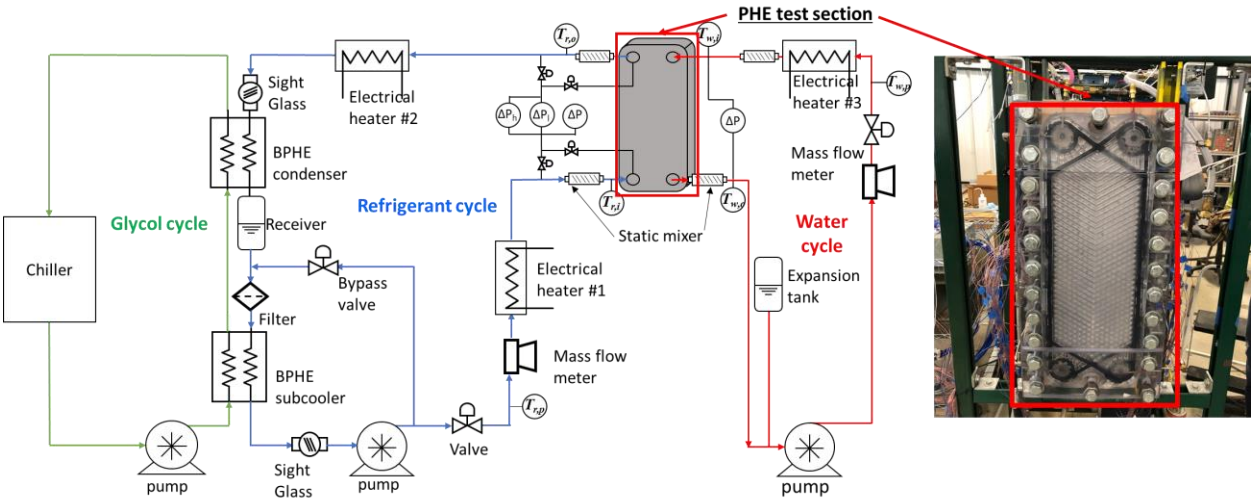


**Figure 5:** Scheme of the experimental setup with a photo of front vies of the test section.

Type T (copper-constantan) thermocouples, absolute and differential pressure transducers, and micromotion flow meter are mounted at locations as marked in Figure 5. Their range and uncertainty after calibration are listed in Table 1. National Instrument SCXI1000 chassis is used for data acquisition. It is connected to a desktop computer through PCI-MIO-16e-1 and used in conjunction with LabVIEW software. The modules and terminal blocks used in the data logger are SCXI1102-SCXI1303 for input measurement and SCXI1124-SCXI1325 for output control. All data are obtained under steady-state conditions for about 30 minutes. Phantom V9.1 high-speed camera is utilized to capture the two-phase flow between the plates.

**Table 1:** Measurement uncertainty

| **Measured Parameter** | **Uncertainty** |
|---|---|
| Temperature (T-type TCs) | 0.1-0.2 °C |
| Absolute pressure 0~2 MPa | 0.25% (full scale) |
| Differential pressure 0~10 kPa | 0.25% (full scale) |
| Mass flow rate 0~150 g/s | 0.1% (reading) |

## 5. RESULTS AND DISCUSSION

The heat transfer and flow visualization were investigated for upward flow boiling of R245fa while being heated from two sides by water, as shown in Figure 1. The first part of this section discusses the validation of the HFM measurements for two-phase flow in a three-channel setup. Furthermore, the results explain how the HTC distribution was obtained from the HFM. Frames of the recorded videos from the visualization method used to link with the HTC variation behavior.

### 5.1 Validation of HFM in Two-Phase Flow

For experimental runs with evaporating R245fa, the heat transferred in the water and refrigerant streams are compared employing the inlet and outlet readings, according to Equations (1) and (2).

$$Q_w = m_w \cdot c_p \cdot \left(T_{w,i} - T_{w,o}\right) \tag{1}$$

$$Q_r = m_r \cdot \left(h_{r,o} - h_{r,i}\right) \tag{2}$$

The average heat flow between the streams of $Q_w$ and $Q_r$ is compared with the heat measured by the HFM. The total heat across the HFM is calculated according to the calibrated local thermal resistance and the measured wall temperature of the plates, according to Equation (3).

$$Q_{HFM} = \sum_{i=1}^{64} A_i \frac{\Delta T_i}{R_i} \tag{3}$$

Where the segmented area $A_i$ is defined according to the location of thermocouples, as shown in Figure 2, and its corresponding thermal resistance $R_i$ obtain from the calibration, as indicated in Figure 3. The temperature difference $\Delta T_i$ assigned for each area is the average of three readings surrounding the triangular spot.

The average heat load of both streams is compared to the heat measured by the HFM in Figure 6(a). The blue asterisk in the figure represents the data obtained from a three-channel setup. Since the HFM is placed on one side of the refrigerant channel, it only measures half of the heat transferred from the heated water. However, in a real situation, the thermal-hydraulic performance cannot be considered identical in each channel (Li and Hrnjak, 2019). The mass flow rate distribution and pressure drop in the channels are Unequitable. Moreover, after the calibration of the HFM, it was realized that the average thermal resistance of the HFM higher than the polycarbonate's thermal resistance. That is also why the measured heat by HFM shows lower values than the heat transfer in the streams. Furthermore, a two-channel setup was implemented for the same comparison. The polycarbonate plate is removed to have one water channel heating the refrigerant channel, separated by the HFM. The black dots in Figure 6 represent data from the 2-channels setup with a 7% percentage difference. The results in the next section are from a three-channel setup. Using the three-channel setup will show us the distribution of the thermal performance and reflect a more realistic condition for the refrigerant channel, where it is being heated from two sides.

The experimental test section is providing qualitative thermal information for plate heat exchangers under realistic conditions. However, the unique HFM instrument in 2 or 3-channels setups as shown in Figure 6(b) requires different water operating conditions (temperature and mass flow rate) than a real industrial PHE, which uses a high number of channels. The high thermal resistance of the HFM requires a higher water temperature to provide the same heat flux to the refrigerant channel. Moreover, in the three channel-setup (or even the two-channel), the water streams provide heat to the refrigerant only from one plate. Away from the endplates in the real heat exchanger, each water channel's capacity is divided between two adjacent refrigerant channels. Therefore, the heat capacity of the water streams is reduced to almost half using 3-channels. This will reflect in either a different mass flux or different temperature difference between the inlet and outlet.

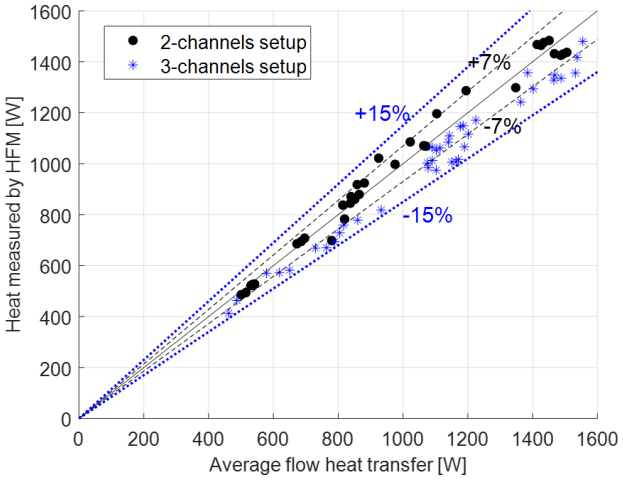


**Figure 6(a):** Energy balance between the streams and the HFM plate

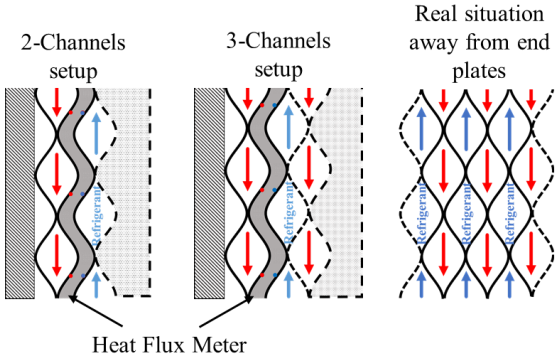


**Figure 6(b):** Different assemblies of PHE using HFM and plates in real PHE

## 5.2 Results and Discussion

R245fa is being evaporated in the test section with a saturation temperature of $T_{sat}$=23.5°C, inlet quality 0.2, outlet quality 0.8, at a mass flux of G=9.6 kg/(m$^2$s). The measurement values obtained from the HFM are two sets of temperatures reading ($T_{wall,w}$ and $T_{wall,r}$) from two plates. The results are displayed with linear interpolation between the points to generate the temperature distribution shown in Figures 7(a & b). The corresponding heat flux $q$ and the heat transfer coefficient distribution $HTC$ are also presented in Figures 7(c & d), respectively, using the Equations (4) & (5).

$$q_i = \frac{\left(T_{wall_w} - T_{wall_r}\right)_i}{R_i}; \quad i = 0...43 \tag{4}$$

$$HTC_i = \frac{q_i}{\left(T_{wall_r} - T_{sat_r}\right)_i}; \quad i = 0...43 \tag{5}$$

Where *i* indicate the number of thermocouples or the reading location, as shown in Figure 2. The refrigerant flow's saturation temperature is calculated from the corresponding pressure measured at the inlet and outlet ports. A local saturation temperature is also considered by assuming a linear pressure drop vertically across the plate.

The highest values are located at the waterside inlet from the two temperature distribution maps, while the lowest at the refrigerant side outlet. These two regions are experiencing an ascendant flow from one side more than another side. For example, the downward flow of water is receded from the left upper area i.e., the refrigerant outlet area, due to the gravitation pull. The refrigerant's upward flow shows a better accumulation at the equivalent region from its side, the plate's right bottom area. As a result, the heat flux shows a critical change in these regions before being uniform in the plate's middle region.

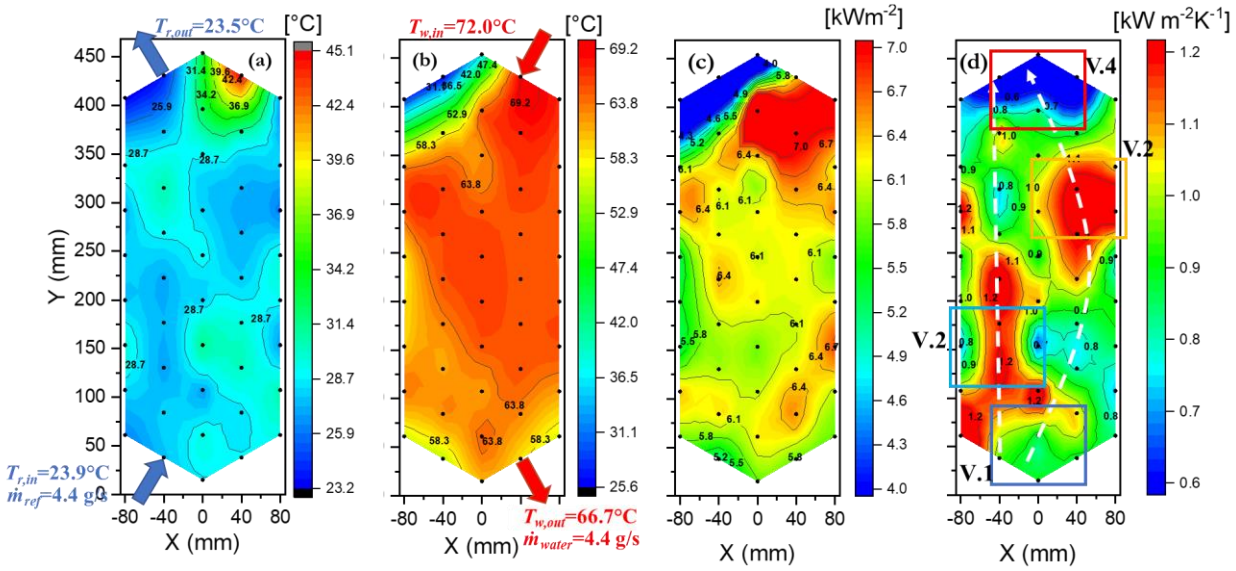


**Figure 7:** Distribution maps of (a) Refrigerant sidewall temperature, (b) water sidewall temperature, (c) heat flux and (d) heat transfer coefficient for R245fa flow boiling

The HTC map from Figure 7(d) is linked and compared to the visualization videos captured, as shown in Figure 8. The distribution area of the PHX faces the most maldistribution of the mass flow rate. As the two-phase flow enters the channel, it tends to flow to a less pressure drop path from inlet to outlet. Thus, it is more likely to flow directly and vertically between the ports, as indicated in the white dashed line in Figure 7(d). However, the plate's corrugated shape that increases the pressure drop by its contact points also enhances the flow to be distributed along the width. Figure 8(a) shows that the vapor phase movements tend to be directed upward to the outlet more than the liquid phase due to their different densities. The light blue line in the figure indicated a boundary of the two regimes noticed. The corrugation shape and contact points influenced the liquid phase more due to their higher viscosity, which caused liquid pooled in the bottom right section. Therefore, the vapor phase's high inertia enhances the HTC in the left region to almost half of the plate. The videos' flow motion showed that the right half was relatively lower compared to the right half. Still, that region received enough heat from the water flows since it's in the water flow outlet to show nucleation behavior.

Even if the flow tends to flow directly to the outlet port, the PHX geometry helps to uniform the mass distribution, causing a portion of the refrigerant to travel through the width, as indicated in the dashed lines of Figure 7(d). Images

in Figure 8(b & c) show a uniform distribution mass flow in the plate's middle regions. The longer path is expected to receive more heat flux from the water channels since it travels through a portion where the water tends to exist more.

Near the outlet upper region, a dry out zone was observed with the lowest HTC recorded. Complete evaporation of the refrigerant achieved from the slower path passes over the highest water temperature causing the dry out region, as shown in Figure 8(d). The orange line indicates approximately the borders of the dry out region. However, the outlet is a mixed flow of two phases. The short straight path did not reach complete evaporation and mixed with the superheated flow before exiting the PHE.

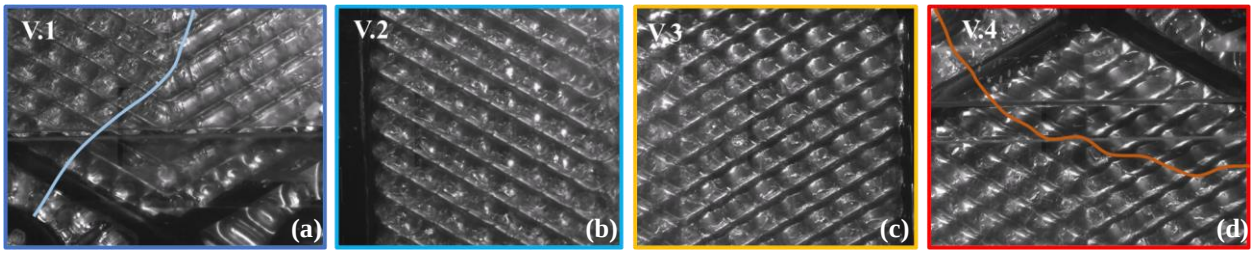


**Figure 8:** Correlating the visualization videos to the measured HTC in Figure 7(d)

The effect of different mass fluxes at $G$=10, 15, and 20 kg/m$^2$s was tested for inlet quality $x_{in}$=0.2 and outlet quality $x_{out}$=0.8-1 at fixed saturation pressure $P_{sat}$=140 kPa. Figure 9 shows the distribution of the HTC for each case with their variation across the vertical direction. As the mass flux increases, the HTC slightly increased, where the average values of the HTC are 0.916, 0.968, and 1.060 kW/(m$^2$K), respectively.

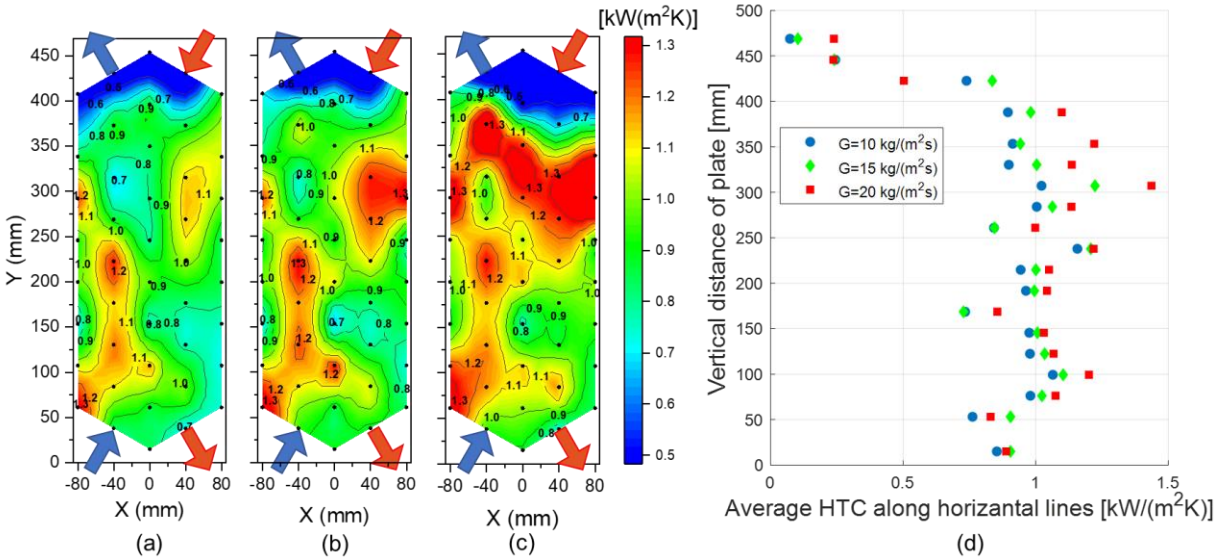


**Figure 9**: Heat transfer coefficient maps for (a)$G$=10 kg/m$^2$s (b)$G$=15 kg/m$^2$s (c)$G$=20 kg/m$^2$s for inlet quality $x_{in}$=02 and $P_{sat}$=140 kPa and their comparison along the vertical direction (d).

However, the HTC variation trend for each case is almost the same; this could mean that the two-phase regime's distribution is the same along with the plate. The HTC values at the dry out region are not affected by different mass fluxes. Still, the mass flux affects the dry out boundaries near the outlet as long as the liquid pooled region near the inlet. Figure 10 shows this behavior from the visualization also. As mass flux increases, the inertia of the flow suppresses the liquid pool region and even results in a larger dry-out region. In the liquid pool region, the nucleation boiling increases as the heat flux from the water channel increases, causing the bubble to flow toward the two-phase region.

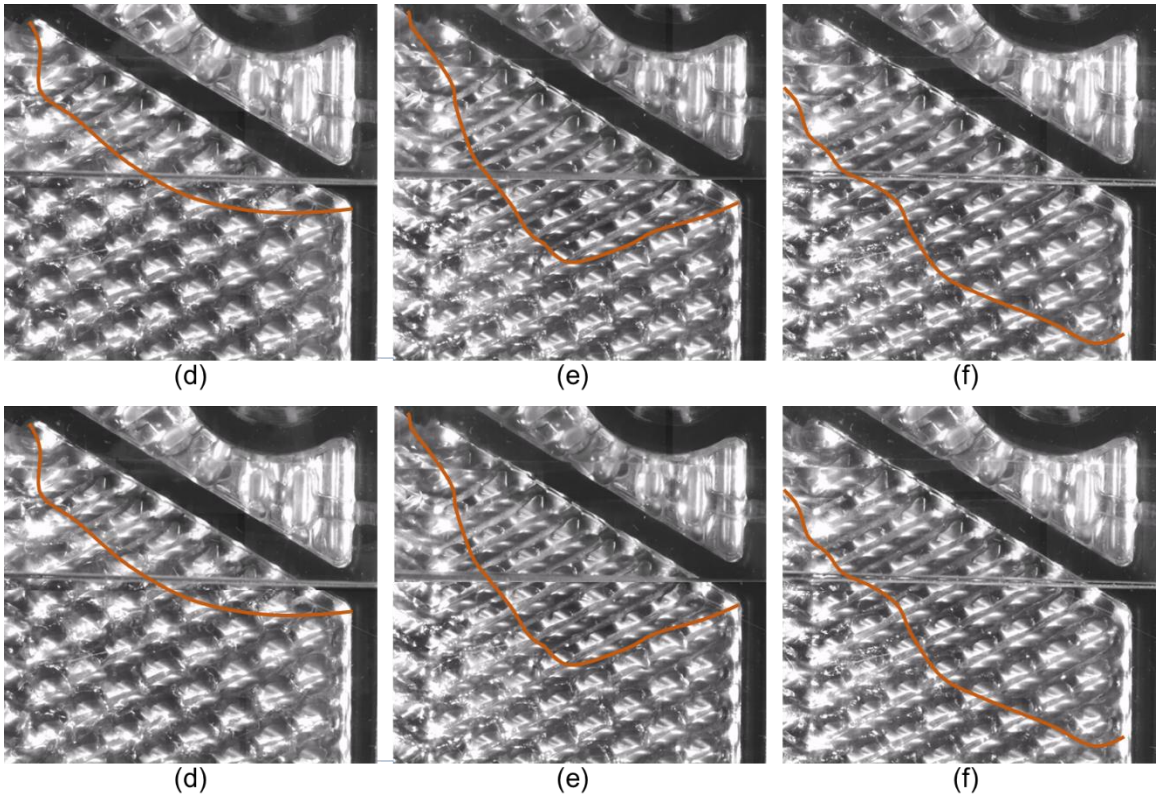


**Figure 10:** Visualization of the liquid pool region for(a)$G$=10 kg/m$^2$s (b)$G$=15 kg/m$^2$s (c)$G$=20 kg/m$^2$s and the dry out region for (d)$G$=10 kg/m$^2$s (e)$G$=15 kg/m$^2$s (f)$G$=20 kg/m$^2$s

## 6. CONCLUSIONS

This paper presented a novel method developed by members of ACRC to combine two-phase flow visualization with simultaneous measurement of local heat transfer coefficient in PHEs. Further and detailed calibration was accomplished for a fabricated heat flux meter (HFM) to increase the measurements' certainty. The HFM substituted one side of the refrigerant channel to measure the HTC. The other side of the refrigerant channel was replaced by two transparent plates to allow visualization access. The low-pressure refrigerant R245fa was heated using two water channels from both sides.

Visualization of flow and corresponding measurements of local temperature, heat flux, and HTC were captured in diabatic realistic conditions (the difference is a smaller number of plates). The flow boiling visualization clearly showed a uniform flow regime and HTC distribution in the middle region of the PHX, even at different mass fluxes. However, a nonuniform flow behavior was observed from visualization near the inlet and the outlet regions. This influenced the HTC that has been measured by the HFM. A liquid pooled region and dry out region were observed in a stream condition with quality varying from 0.2 at the inlet to less than 1 at the outlet. The plate's width and corrugation pattern cause a separation of flows and phase as the two-phase inlet enter. A higher mass flux tends to play a significant role in changing these two regions. A higher mass flux suppresses the pooled region's boundaries and enhances the HTC at the inlet region. Also, the average value of the HTC and even the local values increases slightly with the mass flux. The dry out region shows almost the same values of HTC at different mass fluxes.

## NOMENCLATURE

| | | |
|---|---|---|
| $\Delta T$ | temperature difference | (K) |
| $c_p$ | specific heat | (J/kg·K) |
| $G$ | mass flux | (kg/m$^2$·s) |
| $h$ | enthalpy | (J/kg) |

| | | | |
|---|---|---|---|
| *HTC* | heat transfer coefficient | ($W/m^2 \cdot K$) | |
| $\dot{m}$ | mass flow rate | (kg/s) | |
| *q* | heat flux | ($W/m^2$) | |
| *Q* | heat transfer rate | (W) | |
| *R* | thermal resistance | ($m^2K/W$) | |
| *T* | temperature | (K) | |
| *x* | quality | (-) | |
| **Subscript** | | | |
| *sat* | saturation | *wall* | at wall surface of plate |
| *h* | hot side | *c* | cold side |
| *i* | inlet | *o* | outlet |
| *w* | water | *r* | refrigerant |

## REFERENCES


Arima, H., Kim, J. H., Okamoto, A., & Ikegami, Y. (2010). Local boiling heat transfer characteristics of ammonia in a vertical plate evaporator. *International Journal of Refrigeration*, *33*(2), 359-370.

Freund, S., & Kabelac, S. (2010). Investigation of local heat transfer coefficients in plate heat exchangers with temperature oscillation IR thermography and CFD. *International Journal of Heat and Mass Transfer*, *53*(19-20), 3764-3781.

Gherasim, I., Galanis, N., & Nguyen, C. T. (2011). Heat transfer and fluid flow in a plate heat exchanger. Part II: Assessment of laminar and two-equation turbulent models. *International Journal of Thermal Sciences*, *50*(8), 1499-1511.

Gherasim, I., Taws, M., Galanis, N., & Nguyen, C. T. (2011). Heat transfer and fluid flow in a plate heat exchanger part I. Experimental investigation. *International Journal of Thermal Sciences*, *50*(8), 1492-1498.

Grabenstein, V., & Kabelac, S. (2012). Experimental and theoretical analysis of the local condensation heat transfer in a plate heat exchanger. In *Journal of Physics: Conference Series* (Vol. 395, No. 1, p. 012169).

Hsieh, Y. Y., Chiang, L. J., & Lin, T. F. (2002). Subcooled flow boiling heat transfer of R-134a and the associated bubble characteristics in a vertical plate heat exchanger. *International Journal of Heat and Mass Transfer*, *45*(9), 1791-1806.

Jassim, E. W., Newell, T. A., & Chato, J. C. (2001). Investigation of adiabatic refrigerant pressure drop and flow visualization in flat plate evaporators. Air Conditioning and Refrigeration Center. College of Engineering. University of Illinois at Urbana-Champaign.

Jin, S., & Hrnjak, P. (2017). A new method to simultaneously measure local heat transfer and visualize flow boiling in plate heat exchanger. *International Journal of Heat and Mass Transfer*, *113*, 635-646.

Li, W., & Hrnjak, P. (2019). Experimental investigations of the single-phase flow distribution in brazed plate heat exchangers and its impact on the heat exchanger. *25th IIR International Congress of Refrigeration, ICR 2019*, 2746-2753. International Institute of Refrigeration.

Solotych, V., Lee, D., Kim, J., Amalfi, R. L., & Thome, J. R. (2016). Boiling heat transfer and two-phase pressure drops within compact plate heat exchangers: Experiments and flow visualizations. *International Journal of Heat and Mass Transfer*, *94*, 239-253.

Vakili-Farahani, F., Amalfi, R. L., & Thome, J. R. (2014). TWO-PHASE FLOW OF R245FA IN A 1MM CORRUGATION DEPTH PLATE HEAT EXCHANGER− PART II: FLOW BOILING HEAT TRANSFER. *Interfacial Phenomena and Heat Transfer*, *2*(4).

Yan, Y. Y., & Lin, T. F. (1999). Evaporation heat transfer and pressure drop of refrigerant R-134a in a plate heat exchanger. *Journal of Heat Transfer*, 118-127.


## ACKNOWLEDGEMENT

The authors would like to thank the Creative Thermal Solutions, Inc. and Air Conditioning and Refrigeration Center at the University of Illinois at Urbana-Champaign for the valuable resources and support. The authors also appreciate the help of the research assistants Akira Nakano and Xinting Wang for their contribution to this work.